Nanoparticles of SnO Produced by Sonochemistry as Anode Materials for Rechargeable Lithium Batteries

Doron Aurbach,* Alex Nimberger, Boris Markovsky, Elena Levi, Elena Sominski, and Aharon Gedanken

Department of Chemistry, Bar-Ilan University, Ramat Gan 52900, Israel

Received February 6, 2002. Revised Manuscript Received July 25, 2002

Nanoparticles of SnO were synthesized sonochemically in mildly basic $SnCl_2$ solutions. The amorphous product thus obtained could be transformed to a nanocrystalline phase by heating to 200 °C. Composite electrodes comprised (by weight) of 80% SnO, 10% graphite flakes (conductive additive), and 10% polymeric binder (an optimal composition) were tested as anodes for rechargeable Li batteries. The nanocrystalline SnO was found to be much more effective as an active material for electrodes than the initial amorphous phase. These electrodes could reach nearly their theoretical capacity (≃790 mAh/g, SnO) in electrochemical lithiation−delithiation processes versus a Li counter electrode in nonaqueous Li salt solutions. However, there is still a long way to go to the possible use of SnO as an anode material in practical batteries. This is due to its high irreversible capacity (Li_2O formation and surface film precipitation due to reactions of lithium−tin compounds with solution species) and gradual capacity decrease during repeated charge−discharge cycling. Possible reasons for this capacity fading are discussed. The tools for this study included electron microscopy (both TEM and SEM), thermal analysis (DSC), XRD, FTIR and impedance spectroscopies, and standard electrochemical techniques.

I. Introduction

The development of high energy density rechargeable lithium batteries has been one of the greatest challenges of modern electrochemistry during the last three decades. However, the use of metallic lithium as an anode in secondary batteries was found to be very problematic. This is due to the fact that there is no way to avoid continuous reactions between highly reactive lithium deposits (formed during charging of a lithium battery) and the solution components.[1] Hence, major problems in rechargeable batteries based on lithium metal anodes are the loss of solution upon charge−discharge cycling that considerably limits the cycle life of these batteries and dendrite formation during Li deposition, which may short the batteries and thus create severe safety problems upon their current use.[2]

Successful alternatives to lithium anodes in rechargeable batteries were found to be lithiated carbonaceous materials, mainly graphite.[3] Indeed, the development of lithiated carbon anodes and lithiated transition metal oxide cathodes (e.g., $LiMn_2O_4$, $LiCoO_2$, $LiNiO_2$), both reversibly inserting lithium into nonaqueous electrolyte solutions, paved the way to the invention and commercialization of rechargeable lithium ion batteries based on the "rocking chair" concept.[4] These batteries, which are now practical and are conquering increasingly more power source markets, can indeed be considered as one of the most impressive successes of the electrochemistry technological community in recent years. However, although changing from lithium metal to lithiated graphite means a gain in stability, safety, and cycle life of rechargeable Li batteries, it is at the expense of loss of capacity (372 mAh/g for fully lithiated graphite, LiC_6, compared with 3800 mAh/g for lithium metal). Thereby, there is a continuous driving force for the development of alternative anode materials for both lithium and lithiated graphite, with which the capacity is much higher than that of lithiated graphite yet the safety features are acceptable (i.e., much better compared with metallic lithium). Natural candidates as alternatives for Li anodes in rechargeable Li batteries are lithium alloys, which can be formed and decomposed electrochemically, reversibly, in nonaqueous electrolyte solutions. Indeed, there are many reports on binary and ternary Li alloys that were tested as Li battery anodes.[5−7]

Of special importance in this respect are the Li−Sn compounds because lithium can be inserted electrochemically, reversibly, into tin to form alloys of high Li content up to $Li_{17}Sn_4$, corresponding to a theoretical capacity of 790 mAh/g.[8] We should mention that the

* Corresponding author. E-mail address: aurbach@mail.biu.ac.il.

(1) Aurbach, D.; Zinigrad, E.; Teller, H.; Dan, P. *J. Electrochem. Soc.* **2000,** *147*, 2486−2493.
(2) Yamaki, J. I.; Tobishima, S. I. In *Handbook of Battery Materials*; Besenhard, J. O., Ed.; Wiley VCH: Weinheim, 1999; Part 3, Chapter 3.
(3) Kinoshita, K. In *Handbook of Battery Materials*; Besenhard, J. O., Ed.; Wiley VCH: Weinheim, 1999; Part 2, Chapter 8.
(4) Winter, M.; Novak, P.; Monier, A. *J. Electrochem. Soc.* **1998**, *145*, 428−436.
(5) Dahn, J. R.; Courtney, I. A.; Mao, O. *Solid State Ionics* **1998**, *111*, 289−294.
(6) Huggins, R. A. In *Handbook of Battery Materials*; Besenhard, J. O., Ed.; Wiley VCH: Weinheim, 1999; Part 4, Chapter 4.
(7) Mohamedi, M.; Lee, S.-J.; Takahashi, D.; Nishizawa, M.; Itoh, T.; Uchida, I. *Electrochim. Acta* **2001**, *46*, 1161−1168.
(8) Winter, M.; Besenhard, J. O. *Electrochim. Acta* **1999**, *45*, 31−50.

10.1021/cm021137m CCC: $22.00
Published on Web 10/01/2002

stoichiometry of the Li−Sn compound was recently revised[9−11] to be $Li_{17}Sn_4$. It appears that insertion of lithium in many alloys, including Li−Sn compounds, is accompanied by pronounced volume changes. These lead to an intrinsic instability of the lithiated alloys in solutions: cracking, loss of passivation, intensive reduction of solution species by the lithiated alloy's surface, and electrical disconnection of active mass due to the formation of surface films.[12]

In recent years, it was suggested that tin oxides (SnO, SnO_2) could be used as precursors for Li−Sn alloys. The lithiated tin alloys are formed while embedded in a Li_2O matrix.[13−15]

$$SnO + 2Li^+ + 2e^- \rightarrow Sn + Li_2O \quad (1)$$

$$SnO_2 + 4Li^+ + 4e^- \rightarrow Sn + 2Li_2O \quad (2)$$

$$Sn + xLi^+ + xe^- \rightarrow Li_xSn\ (0 < x < 4.25) \quad (3)$$

It should be noted that reexamination of the mechanism of the SnO reaction with lithium by several research groups[16−19] lead these authors to the conclusion that some oxygen is retained in the immediate coordination environment of tin. Thereby, lithium is inserted into the Li−Sn−O regions. A detailed description of the Li insertion/deinsertion with SnO appears in some recent papers.[9,20]

While the use of tin oxides as precursors obviously adds a considerable irreversible capacity, required for the formation of Li_2O, the formation of Li−SnO matrixes seems to stabilize the repeated formation of the lithiated alloys.[21,22] It was also found that as the active mass of these systems is comprised of smaller particles, they perform better as anode materials for rechargeable batteries in terms of stability during charge−discharge (lithiation−delithiation) cycling.[23]

Large absolute volume changes can be avoided when the size of the metallic host particles is kept small. In this case, even large volume expansion of the particles does not crack them, as their absolute changes in dimensions are small enough.

The aim of this work was to exploit sonochemistry as a source for producing nanoparticles of SnO and to test sonochemically synthesized tin oxide as an anode material for rechargeable Li batteries. It is well-known from many previous studies that the use of ultrasound radiation in the synthesis of materials leads to the formation of nanoparticles because of the cavitation phenomenon, which characterizes sonochemical reactions in solutions.[24−27] The huge cooling rates ($>10^{12}$ K/s) obtained in sonochemistry yield amorphous products.

We believe that sonochemistry may provide efficient and cheap routes for the synthesis of electrode materials for Li ion batteries, especially when the use of nanoscopic phases is important. For the characterization of the materials and electrodes, we used tunneling and scanning electron microscopies (TEM, SEM), differential scanning calorimetry (DSC), X-ray diffraction (XRD), FTIR spectroscopy, and electrochemical techniques, including fast and slow scan rate voltammetry, chronopotentiometry, and impedance spectroscopy (EIS). We examined the difference in the electrochemical behavior of nanoamorphous and nanocrystalline SnO electrodes and compared their performance with those of electrodes based on commercial SnO material.

II. Experimental Section

The SnO nanoparticles were prepared by a sonochemical method as follows: stoichiometric mixtures of $SnCl_2 \cdot 2H_2O$ and a weak base such as azodicarbamide ($H_2NCON{=}NOCNH_2$) were dissolved in distilled water (70 mL). The aim of the weak base was to maintain a basic environment, which facilitates precipitation of tin oxide (a similar function could also be achieved by the use of NH_3). This solution was sonicated for 2 h under a mixture of Ar + H_2 (5%). The sonication was carried out using a titanium horn (Vibracell, 20 kHz, 100 W cm^{-2}) immersed in solution. During sonication, the temperature was kept at 50 °C. The final product was washed a few times with distilled water and absolute ethanol and dried overnight under vacuum. The as-prepared material was amorphous and nanosized. The crystallization of the as-prepared material was carried out by its annealing at 200 °C under a nitrogen flow for 2−4 h.

The SnO nanoparticles were characterized by XRD (Advance D8 system from Bruker, Inc.), SEM (ISM 840 JEOL, Inc.), TEM (TEM 1220 JEOL, Inc.), differential scanning calorimetry (DSC) and thermogravimetric analysis (TGA) using Mettler Toledo, Inc., system models DSC25 and TGA/SDTA 851, respectively, and FTIR (Magna 860 FTIR spectrometer from Nicolet, Inc., diffuse reflectance mode). The SnO nanoparticles' surface area was measured by nitrogen adsorption (BET approach) using a surface area analyzer model 2375 Gemini from Micromeritics, Inc., and it was around 20 m^2/g.

Composite electrodes were comprised of 80% active mass (SnO), 10% carbonaceous additive (carbon black or graphite KS-6 from Timrex, Inc.), 10% poly(vinylidene difluoride)

(9) Goward, G. R.; Leroux, F.; Power, P.; Ouvrard, G.; Dmowski. W.; Egami, T.; Nazar, L. F. *Electrochem. Solid State Lett.* **1999**, *2* (8), 367−370.
(10) Wang, Y.; Sakamoto, J.; Huang, C.-K.; Surampudi, S.; Greenbaum, S. G. *Solid State Ionics* **1998**, *110*, 289−294.
(11) Courtney, I. A.; Dunlap, R. A.; Dahn, J. R. *Electrochim. Acta* **1999**, *45*, 51−58.
(12) Huggins, R. A. *Solid State Ionics* **1998**, *113−115*, 57−67.
(13) Brousse, T.; Retoux, R.; Herterich, H.; Schleich, D. M. *J. Electrochem. Soc.* **1998**, *145*, 1−4.
(14) Chouvin, J.; Branci, C.; Sarradin, J.; Olivier-Fourcade J.; Jumas, J. C.; Simon, B.; Biensan, Ph. *J. Power Sources* **1999**, *81−82*, 277−281.
(15) Wang, C.; Appleby, A. J.; Little, F. E. *J. Power Sources* **2001**, *93*, 174−185.
(16) Chouvin, J.; Olivier-Fourcade, J.; Jumas, J. C.; Simon, B.; Biensan, Ph.; Fernandez Madrigal, F. J.; Tirado, J. L.; Perez Vicente, C. *J. Electroanal. Chem.* **2000**, *494*, 136−146.
(17) Hightower, A.; Delcroix, P.; Le Caër, G.; Huang, C.-K. V.; Ratnakumar, B. V.; Ahn, C. C.; Fultz, B. *J. Electrochem. Soc.* **2000**, *147*, 1−8.
(18) Mansour, A. N.; Mukerjee, S.; Yang, X. Q.; Mcbeen, J. *J. Electrochem. Soc.* **2000**, *147*, 869−873.
(19) Wang, Y.; Sakamoto, J.; Kostov, S.; Mansour, A. N.; den Boer, M. L.; Greenbaum, S. G.; Huang, C.-K.; Surampudi, S. *J. Power Sources* **2000**, *89*, 232−236.
(20) Goward, G. R.; Taylor, N. J.; Souza, D. C. S.; Nazar, L. F. *J. Alloys Compd.* **2001**, *329*, 82−91.
(21) Idota, Y.; Kubota, T.; Matsufuji, A.; Maekawa, Y.; Miyasaka, T. *Science* **1997**, *276*, 1395−1397.
(22) Courtney, I. A.; Dahn, J. R. *J. Electrochem. Soc.* **1997**, *144*, 2045−2052.
(23) Winter, M.; Besenhard, J. O.; Spahr, M. E.; Novak, P. *Adv. Mater.* **1998**, *10*, 725−763.
(24) Zhu, J.; Lu, Z.; Aruna, S. T.; Aurbach, D.; Gedanken, A. *Chem. Mater.* **2000**, *12*, 2557−2566.
(25) Suslik, K. S.; Price, G. J. *Annu. Rev. Mater. Sci.* **1999**, *29*, 295−326.
(26) Dhas, N. A.; Gedanken, A. *Chem. Mater.* **1997**, *9*, 3159−3163.
(27) Jeevanandam, P.; Koltipin, Y.; Gedanken, A.; Mastai, Y. *J. Mater. Chem.* **1997**, *10*, 2143−2146.

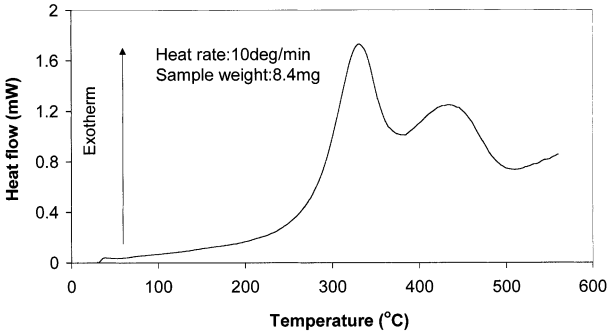

Figure 1. DSC curve of the as-prepared tin oxide powder (an amorphous phase).

(PVdF) binder (Solvey, Inc.), and a copper foil current collector. The powder mixtures (active mass, carbon, and binder) were softly milled for 20 min with a Crescent Wig L-Bug 3110B amalgamator. The weight ratio between the steel ball (6.35 mm in diameter) and the powder was 4:1. The powder mixtures obtained were then dissolved in *N*-methylpyrollidone to make a slurry that spread uniformly on both sides of a 0.125 mm thick copper foil (GoodFellow, 99.8%) current collector and were dried overnight in a vacuum at 120 °C. The active mass of the electrodes was 2−3 mg/cm^2. Some of the electrodes were pressed (3 ton/cm^2). For comparison, we prepared and studied electrodes based on commercial SnO material (powder from Merck KGaA). The latter comprised irregular-shaped particles of micronic size (5−50 μm). Three-electrode cells (parallel plate configuration, with Li strip and Li foil reference and counter electrodes) were used for the electrochemical characterization. All the electrochemical measurements, as well as the preparation for the spectroscopic and morphological studies, were carried out under a highly pure argon atmosphere (O_2 and H_2O level less than 5 ppm) in VAC, Inc., gloveboxes.

The electrolyte solution was 1 M $LiPF_6$ (Hashimoto, Inc.) in a 1:1 mixture of ethylene carbonate (EC) and dimethyl carbonate (DMC) from Merck KGaA, and EC/DMC (1:3, Merck KGaA)/1 M $LiAsF_6$ (Lithco, Inc.). Cyclic voltammetry was measured using a Solartron (Model BTU 1470) potentiostat, driven by the Cell Test (Solartron, Inc.) software, or an EG&G potentiostat (Model 273), driven by the Corrware (Scribner, Inc.) software. Electrochemical impedance spectroscopy (EIS) measurements were carried out in the 25 kHz to 10 mHz frequency range and at a 3 mV ac amplitude using the Solartron Inc. model 1286 electrochemical interface or the Model BTU 1470 multichannel potentiostat and model 1255 frequency response analyzer. Galvanostatic cycling was performed using a computerized multichannel Maccor-2000 battery tester. All experiments were carried out at 25 °C in thermostats.

III. Results and Discussion

Sonochemical synthesis of the SnO provides nanoparticles of an amorphous material. Upon heating to 200 °C, the material is transformed to nanocrystals. Further heating above 350 °C leads to disproportionation of the tin oxide, a well-known reaction,[28] according to the following equation:

$$2SnO \rightarrow Sn + SnO_2 \qquad (4)$$

This thermal behavior of the sonochemically synthesized tin oxide is demonstrated in Figure 1, which shows a typical thermogram obtained by the DSC measurements. The thermogram has the two exothermal peaks related to the phase transition (onset > 200 °C, peak around 325 °C) and to the decomposition (around 425 °C) of the material. The shape of the thermograms obtained from these processes and the peaks' locations depend, of course, on the heating rate.

Figure 2 compares TEM micrographs of the amorphous (a) and the nanocrystalline (b) SnO materials, which clearly show nanoparticles at different morphologies, related to the two phases. The sizes of the nanoparticles estimated from the TEM measurements are indicated in this figure.

We compared the XRD patterns of the nanocrystalline powder soon after preparation and a powder that was in contact with air for a few months. The XRD pattern of the pristine annealed material is indeed typical of SnO, while the material that was exposed to air shows XRD patterns of tin dioxide[29] in addition to the SnO peaks. Hence, the SnO active mass has to be stored under inert atmosphere, since contact with air leads to its oxidation to SnO_2 (high surface area due to the nanoscopic size of the particles).

To explore the electrochemical behavior of the SnO as an anode material for rechargeable Li batteries, we have optimized our working system (electrode, electrolyte solution) taking into account the following relevant parameters: (1) active mass (amorphous or crystalline nanophase), (2) conductive additive (graphite or carbon black), (3) the amount of binder and conductive additive, (4) the electrodes' morphology in terms of their compactness (pressed or unpressed), (5) electrolyte solution (Li-salt used: $LiPF_6$ or $LiAsF_6$).

Then, to obtain integrated and homogeneous composite electrodes with an optimal electrical contact within the active mass and adhesion to the current collector, it was necessary to mix the components using mild milling before the electrodes' preparation.

The screening tests were galvanostatic cycling in two-electrode cells (a composite working electrode vs a lithium foil counter electrode). The major parameters of interest here were the capacity in the lithiation−delithiation processes of the electrodes and its decay upon cycling.

From these experiments, it was clear that the nanocrystalline material is superior to the amorphous phase; graphite particles are much better than carbon black powder as conductive additives for the composite electrodes. It was also established that using unpressed electrodes and $LiPF_6$/EC−DMC electrolyte solution demonstrated better cycleability and lower capacity fading. This finding is surprising, as it was clearly demonstrated previously that, for Li secondary Li-metal or lithiated graphite anodes, $LiAsF_6$ is the best salt to be used in the electrolyte solutions, for reasons related to the complicated surface chemistry developed in these systems (which determines their electrochemical behavior).[30,31]

Consequently, we concentrated on the study of unpressed composite electrodes comprised of nanocrystalline SnO active mass and synthetic graphite flakes as

(28) Courtney, I. A.; Dahn, J. R. *J. Electrochem. Soc.* **1997**, *144*, *2943*−2948.

(29) Sneed, M. C.; Brasted, R. C. *Comprehensive Inorganic Chemistry, V 7, The Elements and Compounds of Group IVa*; New York and Toronto, 1958; XRD of SnO, JCPDS-ICDD, p 6-0395.

(30) Markovsky, B.; Aurbach, D.; Levi, M. D. *Electrochim. Acta* **1998**, *43*, 2287−2304.

(31) Aurbach, D.; Zaban, A.; Chusid, O.; Weissmann, I. *Electrochim. Acta* **1994**, *39*, 51−71.

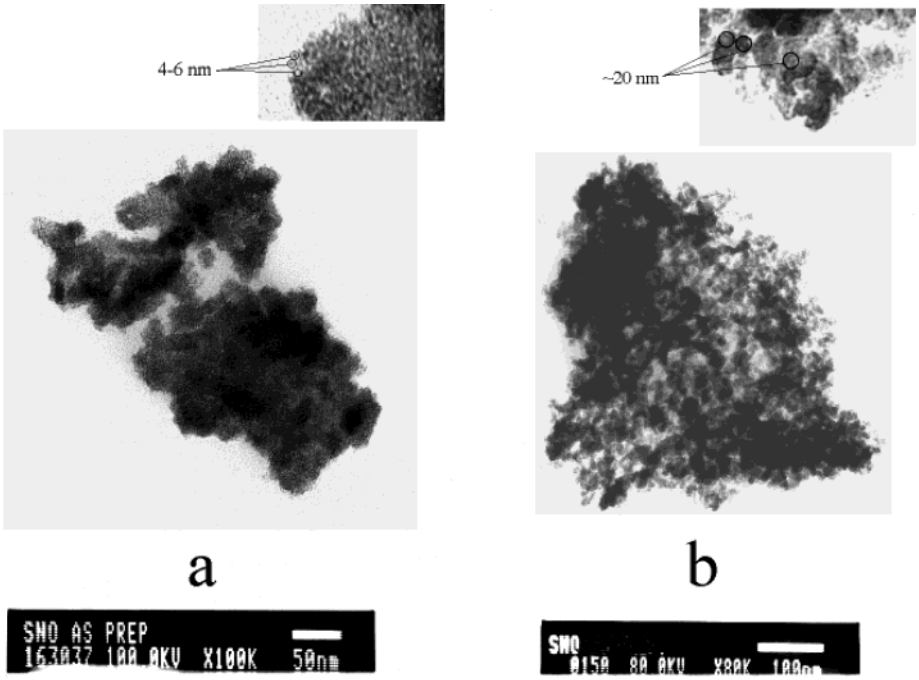

Figure 2. TEM micrographs of tin oxide powders: (a) as-prepared amorphous phase; (b) nanocrystalline phase. Scale bars appear on each micrograph.

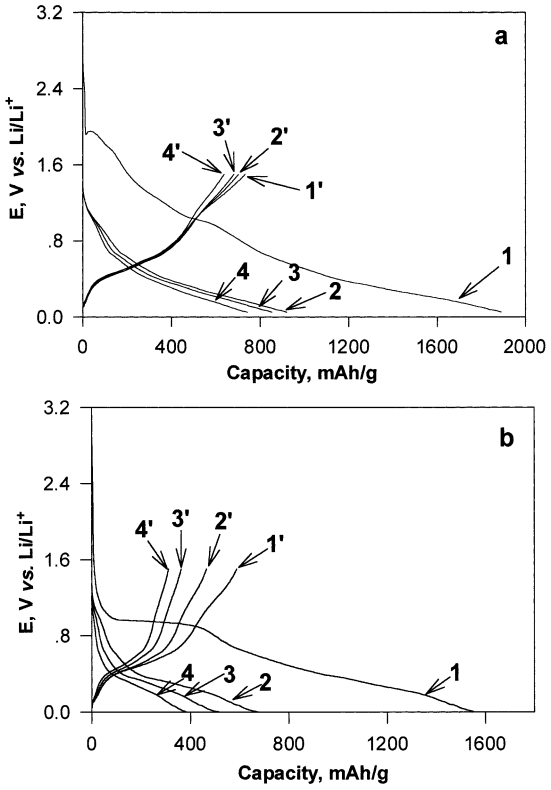

Figure 3. Results of galvanostatic lithiation−delithiation cycling of optimized composite SnO electrodes at C/10 rate in an EC/DMC (1:1)/1 M $LiPF_6$ solution: (a) electrode based on the SnO nanoparticles; (b) electrode based on a commercial SnO material (Merck KGaA). The number of charge−discharge cycles is indicated.

the conductive additive in $LiPF_6$/EC−DMC electrolyte solutions. The optimal composition of the electrodes was found to be 80 wt % active mass (SnO crystalline nanoparticles), 10% PVdF binder, and 10% conductive KS-6 graphite particles.

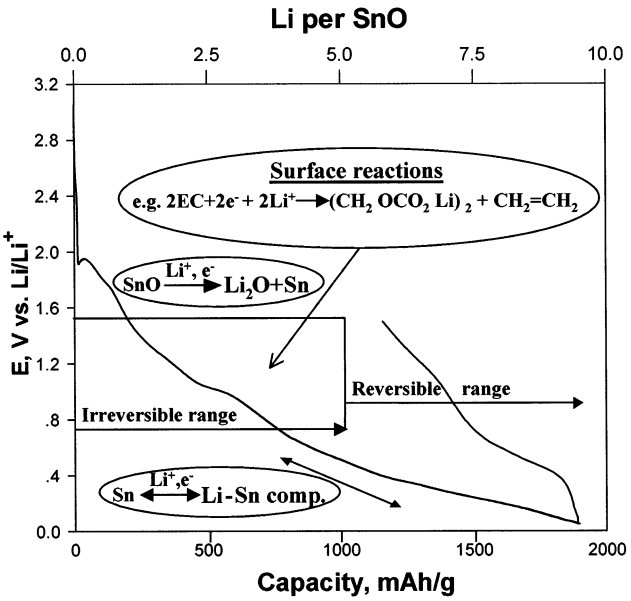

Figure 4. Chronopotentiogram of the first galvanostatic cycle (C/10 rate) of an optimized composite SnO electrode based on nanoparticles in an EC/DMC (1:1)/1 M $LiPF_6$ solution.

Figure 3a shows results of galvanostatic lithiation−delithiation cycling (C/10 rate) of an optimized composite SnO electrode in EC−DMC/$LiPF_6$ solution. Figure 3b represents results of galvanostatic lithiation−delithiation cycling (C/10 rate) of the electrode based on commercial SnO material (80%), 10% graphite, and 10% PVdF. It is spectacular that the electrode based on the nanophase SnO demonstrates higher specific charge and lower capacity fading upon cycling.

Figure 4 shows a chronopotentiogram with an ideal voltage profile of a SnO electrode upon lithiation (thus forming Li_2O and $Li_{17}Sn_4$), which is similar to results of others.[8,12] In the first galvanostatic lithiation process, we obtained capacity of about 1800 mAh/g, while the

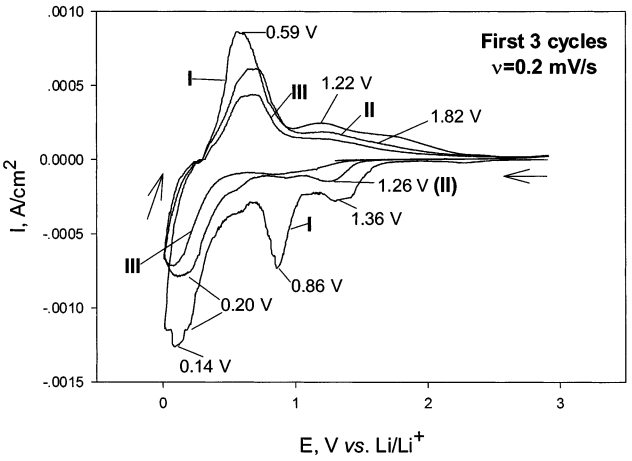

Figure 5. First three cyclic voltammograms recorded at 0.2 mV/s of an optimized composite SnO electrode based on nanoparticles. The electrolyte solution was EC/DMC (1:1)/1 M $LiPF_6$. Numbers of the CVs and relevant peak potentials are indicated.

first delithiation process involves about 850 mAh/g, which is close to the theoretical capacity. The difference—the irreversible capacity around 1000 mAh/g—is due to the following processes: (i) formation of Li_2O and (ii) irreversible reactions of the lithiated composite electrode with solution species. In these reactions, solvent molecules and salt anions are reduced on the active surface, thus forming insoluble Li salts that precipitate as passivating surface films.

Three first cyclic voltammograms (scanning rate 0.2 mV/s) of the optimized composite SnO electrode are presented in Figure 5. In the first CV, a cathodic peak appears at a potential of $E = 860$ mV, which can be attributed to the irreversible reactions which form surface films. This peak does not appear in the subsequent voltammetric cycles. Hence, the first CV cycle can be considered as a "formation" cycle, and then the electrode demonstrates quite a reversible behavior. A pair of cathodic and anodic peaks at 1.26 and 1.82 V can be ascribed to the process of Sn formation according to the reaction in eq 1 (see Introduction), which is considered to be reversible to some extent.[7] The cathodic peaks at 0.20 and 0.14 V can be attributed to the process of alloying of tin with lithium. Our data are in good agreement with the results obtained by other groups.[7]

Figure 6 compares FTIR spectra of powders scraped from pristine and cycled electrodes (diffuse reflectance mode). The spectrum of the pristine material has a pronounced band between 500 and 550 cm^{-1}, which we attribute to SnO. The spectrum of cycled electrodes is rich in IR absorption of surface species. Peaks around 1600−1700, 1470, 1390, 1316, and 1100 cm^{-1} should be attributed to $ROCO_2Li$ species, the alkyl carbonate solvent reduction products on lithium metal, lithiated carbons, and nonactive metal electrodes polarized to low potentials.[32−34]

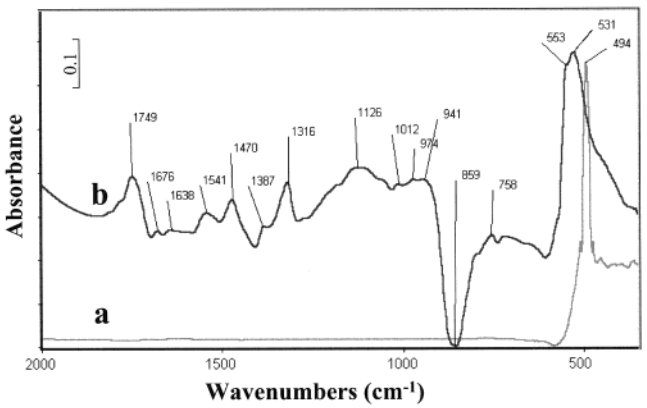

Figure 6. FTIR spectra (diffuse reflectance mode) obtained from powders scraped from composite electrodes comprised of a nanocrystalline tin oxide, a graphite additive, and a PVdF binder: (a) a pristine electrode; (b) an electrode after prolonged cycling (C/10 rate) in an EC/DMC (1:1)/1 M $LiPF_6$ solution.

There are three additional features in the spectra of cycled electrodes, which deserve special discussion. The pronounced IR peak around 1750 cm^{-1} may be attributed either to polycarbonate, a possible polymerization product of EC,[35] or to a trace of EC that could not be washed out of the porous composite electrodes when being prepared for the spectral studies (ex situ, washed powders, in diffuse reflectance mode).

The pronounced peak around 550−530 cm^{-1} in the spectra of the cycled electrode is attributed to SnO (compare to the spectrum of the pristine electrode).

On the basis of XRD patterns of cycled electrodes (see later), there is no bulk SnO left after lithiation of the electrodes and their charge−discharge cycling. Hence, we attribute the pronounced peak around 550−530 cm^{-1} to surface SnO formed by surface oxidation of the tin particles in the electrode, due to unavoidable exposure of the electrode to air during the spectral measurements.

Another interesting feature is the inversed peak around 860 cm^{-1}. It is generally known that species adsorbed to insulating surfaces in monolayers may show inversed IR peaks in the absorbance mode.[32] Usually, the surface films formed on lithiated carbon in $LiPF_6$ solutions contain species of the Li_xPF_y and Li_xPOF_y type, which have pronounced IR bands that belong to the P−F bonds around 850 cm^{-1}.[32−34] It is expected that the above Li_xPF_y species are also formed on the lithiated tin by reduction of the PF_6^- anion, as happens on Li or Li−C surfaces. Hence, we suggest that the inversed peak around 860 cm^{-1} reflects the formation of surface species with P−F bonds due to reduction of the salt anion. The spectral results discussed above are similar to those obtained by others who also studied the surface chemistry of tin oxide anodes.[37]

The presence of surface films, which influence the electrode's kinetics, is reflected by the impedance measurements of these electrodes. In Figure 7, we present impedance spectra obtained from the nanocrystalline SnO electrode at OCV conditions ($E = 1.6$ V). The

(32) Aurbach, D.; Zaban, A.; Ein-Eli, Y.; Weissman, I.; Chusid, O.; Markovsky, B.; Levi, M. D.; Levi, E.; Schechter, A.; Granot, E. *J. Power Sources* **1997**, *86*, 91−98.

(33) Aurbach, D.; Markovsky, B.; Levi, M. D.; Levi, E.; Schechter, A.; Moshkovich, M.; Cohen, Y. *J. Power Sources* **1999**, *81−82*, 95−111.

(34) Aurbach, D.; Markovsky, B.; Weissman, I.; Levi, E.; Ein-Eli, Y. *Electrochim. Acta* **1999**, *45*, 67−86.

(35) Yazami, R. *Electrochim. Acta* **1999**, *45*, 87−97.

(36) Hoffman, H.; Mayer, U.; Krischanitz, A. *Langmuir* **1995**, *11*, 1304−1312.

(37) Li, J.; Li, H.; Wang, Zh.; Huang, X.; Chen, L. *J. Power Sources* **1999**, *81−82*, 346−351. Li, J.; Li, H.; Wang, Zh.; Chen, L.; Huang. X. *J. Power Sources* **2002**, *107*, 1−4.

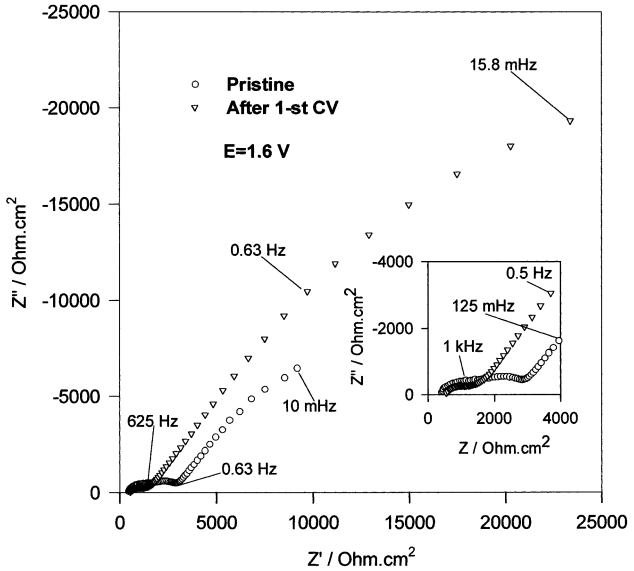

Figure 7. Impedance spectra (Nyquist plots) measured at OCV E = 1.6 V from a pristine SnO electrode based on nanoparticles and from the same electrode after a lithiation−delithiation cycle.

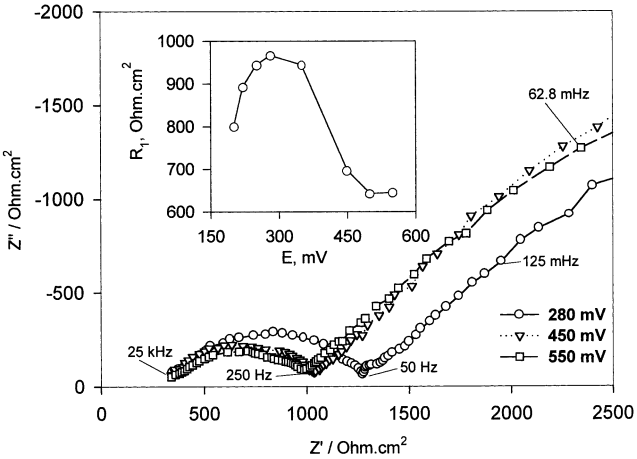

Figure 8. Family of impedance spectra presented as Nyquist plots measured at selected equilibrium potentials (indicated) after a few lithiation−delithiation cycles of the SnO electrode based on nanoparticles. Inset: the variation of the superposition of the resistance of the surface films and charge-transfer resistance calculated from the diameter of the high-to-medium-frequency semicircle as a function of the electrode's potential.

spectrum of the pristine electrode consists of two depressed semicircles at high- and medium-frequency domains, respectively, and an arc at low frequency (0.63 Hz to 10 mHz) region. The impedance of the pristine composite SnO electrode is related mainly to the particle-to-particle interactions and to the initial charge-transfer resistance of the active mass and the relevant interfacial capacitance. The formation of the surface films (comprising lithium alkyl carbonate, Li_2CO_3, and fluorine-containing species, as proved by FTIR studies) during the first cycle leads to a huge increasing of the electrode impedance (medium-to-low-frequency domain in the Nyquist plots).

Figure 8 represents a family of impedance spectra (Nyquist plots) of an electrode after a few lithiation−delithiation cycles, which were measured at selected equilibrium potentials, as indicated. As can be seen, high-frequency semicircles and low-frequency straight lines, typical of "Warburg" type elements, characterize the spectra.[38] Hence, we suggest that three major processes influence the impedance of the lithiated SnO electrodes, namely lithium ion migration through the surface films, charge transfer at the surface films/active mass interface, and solid-state diffusion of lithium in the Li−Sn or Li−Sn−O compounds. We have found that the impedance component, which reflects a superposition of surface film resistance (R_{sf}) and charge-transfer resistance (R_{ct}), is potential-dependent. This impedance (calculated from the diameter of the semicircle in the high-frequency domain of the spectra) is potential-dependent. The dependence of this combined resistance (R_1) on the electrode's potential is presented in the inset in Figure 8. An interesting finding is that a maximum in R_1 around 300−350 mV corresponds to a maximum in the lithium content in the Li−Sn compounds.[12]

Figure 9 presents a comparison of impedance spectra (presented as Nyquist plots) of the fully lithiated composite tin oxide electrode ($Li_{17}Sn_4$ + Li_2O), a lithiated graphite electrode (LiC_6), and a lithium electrode in alkyl carbonate solutions, as indicated. (The identity of the salt is not important for this specific comparison.) The high-frequency part of the spectra from the three electrodes is very similar. As already discussed in detail,[39,40] the high-frequency semicircle in the spectra of lithium and lithiated graphite electrodes is attributed to Li ion migration through the passivating surface films that cover these electrodes.

Hence, the semicircles in the spectra of Figure 8 should also be attributed to Li ion migration through the surface films formed by reduction of solution species on the $Li_{17}Sn_4$ compounds (sufficiently low potentials), which were analyzed by FTIR spectroscopic studies (Figure 6). The potential variation of the resistance of these films (reflected by the changes in the semicircle's diameter as a function of the electrode's potential) may result from the pronounced volume changes of the active mass as Li is inserted and alloyed with tin.[8,12] These changes, which stretch the films, may change their electrical properties. A somewhat similar potential dependence of the surface film's resistance on a graphite electrode was observed and discussed,[41,42] and it may also result from changes in volume as Li is inserted into graphite.

The very high impedance of the surface films of the SnO electrodes on the order of thousands of ohms per square centimeter (seen in Figure 8) is due to the fact that, in $LiPF_6$ solutions, the surface films contain a high concentration of LiF (due to salt anion reduction).[31,39] In the medium-to-low-frequency domain, the impedance behavior of the three electrodes presented in Figure 9 is very different. In the case of lithium electrodes where the redox reaction is mainly lithium deposition−dissolution on the electrode's surface, the low-frequency

(38) Bard, A. J.; Faulkner, L. R. *Electrochemical Methods. Fundamentals and Applications*; John Willey and Sons: New York, 1980; pp 323−336.
(39) Zaban, A.; Zinigrad, E.; Aurbach, D. *J. Phys. Chem.* **1996**, *100*, 3089−3101.
(40) Aurbach, D.; Levi, M. D. *J. Phys. Chem. B* **1997**, *101*, 4630−4640.
(41) Aurbach, D.; Levi, M. D.; Lev, O. *J. Appl. Electrochem.* **1998**, *28*, 1051−1059.
(42) Aurbach, D.; Gnanaraj, J. S.; Levi, M. D.; Levi, E.; Salitra, G.; Fischer, J. F.; Claye, A. *J. Electrochem. Soc.* **2001**, *148*, A525−A536.

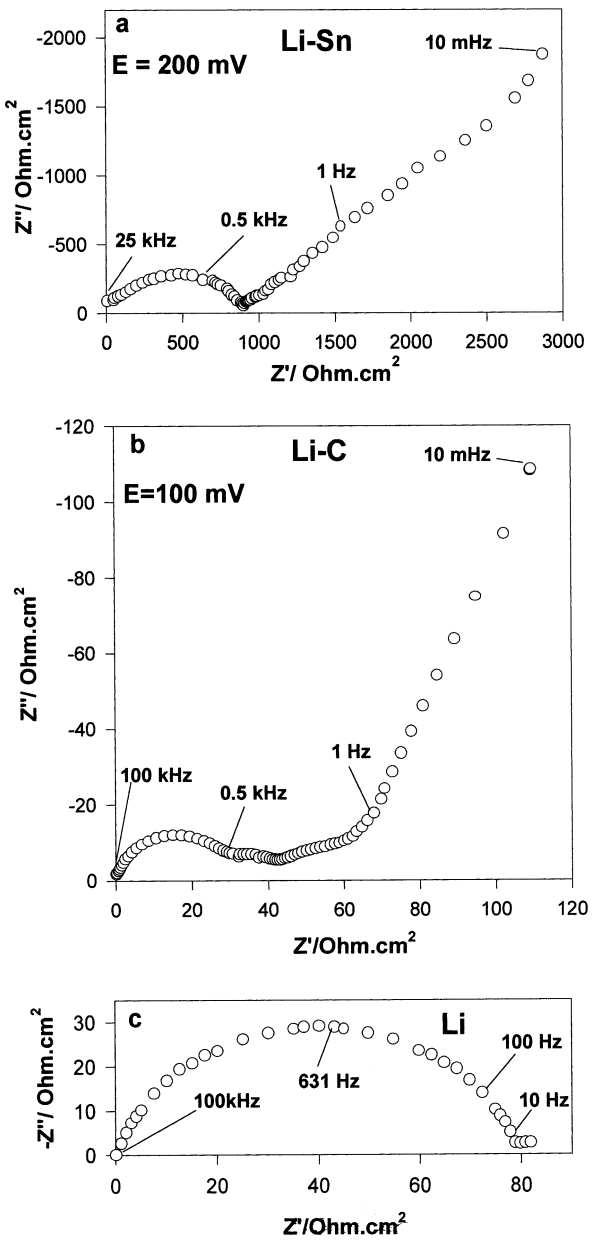

Figure 9. Comparison of typical impedance spectra of the following electrodes: (a) a composite tin oxide electrode after prolonged cycling at a fully lithiated state (nanocrystalline SnO, graphite and PVdF, $LiPF_6$ solution); (b) a lithiated graphite electrode. The electrolyte solution was EC/DMC (1:3)/1 M $LiAsF_6$; (c) a Li metal electrode after 6 days of storage in EC/DEC (1:1)/1 M $LiAsF_6$ (The salt used is not important for this comparison).

impedance is rather low. For the case of graphite, the spectra at the medium-to-low-frequency reflect interfacial charge transfer (surface film/active mass), solid-state diffusion, and phase transition at $\omega \rightarrow 0$ (accumulation of Li in the bulk carbon).[41,42] In the case of the SnO electrodes, the low-frequency part, which looks like a typical "Warburg" type element, probably reflects the diffusion of lithium into the Li−SnO compound. It should be noted that a discussion of the exact mechanism of transport of Li ions and electrons in the solid matrix (Li−Sn−O) is beyond the scope of this paper. The difference in the spectra of SnO electrodes before and after lithiation, measured at a relatively high potential (E = 1.6 V, see Figure 7), should be attributed to their

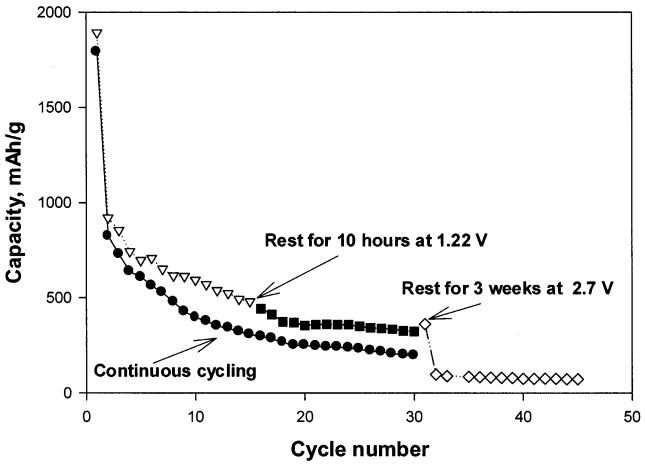

Figure 10. Capacity vs cycle number plots (C/10 rate) obtained from the optimized SnO nanoparticles electrodes in an EC/DMC (1:1)/1 M $LiPF_6$ solution during continuous and interrupted cycling. The events of interruption and their duration are indicated.

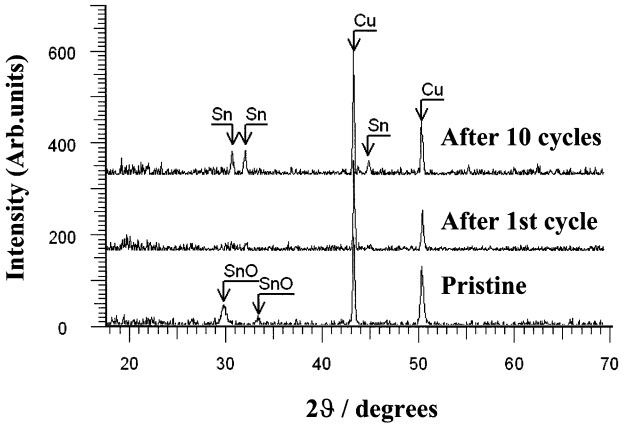

Figure 11. XRD patterns measured from a pristine composite nanocrystalline SnO electrode, a similar electrode after the first lithiation−delithiation cycle (C/10 rate), and a similar electrode after 10 repeated cycles (C/10 rate). EC/DMC (1:1)/1 M $LiPF_6$ solution.

different states in terms of the nature of the surface films and the possible redox reactions (lithiation of SnO vs lithiation of Sn metal). Hence, the irreversible capacity measured and the spectral studies clearly show that, during the first lithiation, the electrodes reduce the major solution components, both solvent molecules and salt anions. The fact that the active mass is a nanoscopic phase with a relatively high surface area should lead to the intensified surface reactions of these electrodes and, hence, to their very high irreversible capacity. The high irreversible capacity of the SnO electrodes due to both the bulk formation of Li_2O and the intense surface reactions is totally unacceptable in rechargeable Li ion batteries, where the Li source is usually the cathode. Therefore, it is clear that preparation of practical SnO anodes for battery application should include a preliminary stage in which the SnO is converted to Sn and Li_2O and the passivating surface films are formed.

Upon charge−discharge cycling of these electrodes, the reversible capacity may be initially very close to the theoretical one, in the first charge−discharge cycles, and then it gradually decays and is stabilized around a few

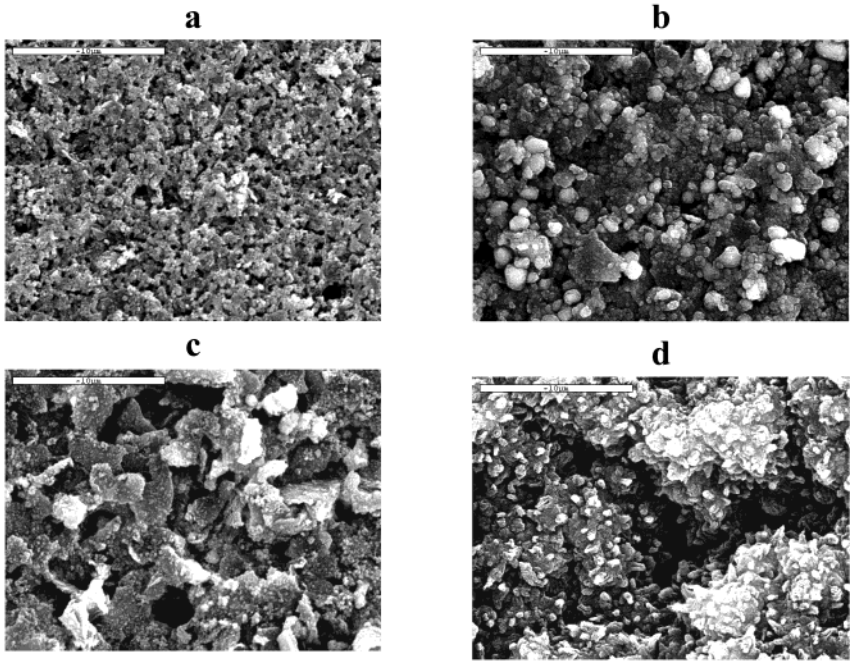

Figure 12. SEM micrographs obtained from a pristine (a and c) and cycled (b and d) composite SnO electrodes: parts a and b relate to an electrode based on SnO nanoparticles; parts c and d relate to an electrode based on micrometer size SnO. EC/DMC (1:1)/1 M $LiPF_6$ solution, C/10 rate. Scale bars appear in each micrograph.

hundred mAh/g (SnO), as seen in Figure 10. It is very significant that when an electrode is cycled in the course of repeated lithiation−delithiation processes and the experiment is then stopped and the electrode remains in solution at open circuit condition for a prolonged time (hours), its reversible capacity decreases considerably (14% after the first rest of 10 h and 70% after the second rest of 3 weeks).

The nature of the lithium insertion process and the $Li_{17}Sn_4$ phases formed depend strongly on the potential window within which these electrodes operate. Hence, limiting the potential window should obviously decrease the capacity of the lithiation process, but it may also stabilize the electrodes' capacity upon cycling. Limiting the potential windows of the charge−discharge processes decreases, as expected, their capacity but does not prevent capacity fading upon cycling. Hence, these electrodes suffer from intrinsic stability problems.

To understand the structural changes of the electrode materials, we compared in-situ XRD patterns of a pristine SnO electrode, an electrode after a first lithiation−delithiation cycle, and an electrode after 10-repeated lithiation−delithiation cycles.

The typical SnO peaks presented in Figure 11, which characterize the pattern of the pristine electrode, are absent in the patterns of the cycled electrodes, which contain, in turn, XRD peaks of metallic tin.

It can be seen that the peaks, which belong to the tin, are weak in the pattern of the electrode after the first discharge−charge cycle, but they are pronounced in the electrode cycled 10 times.

These results confirm that all the SnO is indeed converted to tin, and hence, all the active mass of the electrode is accessible to the electrochemical process, which correlates well with the high reversible capacity (close to the theoretical one) obtained initially with these electrodes.

These XRD data also seem to indicate that, initially, the nanoscopic tin oxide particles are converted upon lithiation−delithiation mainly to an amorphous phase of tin. However, upon cycling, some structural changes take place and the delithiated tin becomes more crystalline.

The morphology differences between the electrodes based on micrometer size (a) and nanoparticles SnO (b) after their prolonged cycling are demonstrated by SEM results (Figure 12). It is spectacular that there are a lot of cracks in the active mass of the cycled electrodes.

The cracks' width was estimated as 1 μm for the nano-SnO and 10−20 μm for the micrometer size SnO electrodes, respectively. The reason for the cracks' creation is the pronounced volume changes[43] of the host material under alloying/dealloying processes.

These cracking phenomena upon cycling indicate problems of integrity of the active mass. Cracking causes obvious problems related to the passivation of these electrodes by stable surface films. It is very likely that part of the active mass becomes isolated by surface films formed on the fresh active surface that the cracks expose, by reactions of Li−Sn compounds and solution components. Thereby, the capacity of the electrodes fades during cycling. On the basis of observations by others,[43] the cracks are formed upon delithiation and are partly closed upon lithiation of the tin, as the volume of the active mass increases. This explains why, in the middle of cycling experiments, electrodes which are stored for a while at open circuit lose capacity faster than electrodes in similar experiments at continuous cycling with no rest: when an electrode is stored in solutions in the highly cracked condition (delithiation), there is a higher chance for detrimental interaction

(43) Beaulieu, Y.; Eberman, K. W.; Turner, R. L.; Krause, K. J.; Dahn, J. R. *Electrochem. Solid State Lett.* **2001**, *4* (9), A137−A140.

between the active mass and the solution species, which leads to electrical isolation of part of the active mass.

All of these experiments clearly show that although from the synthetic point of view we have obtained very promising Li battery anode material, there is a lot of practical engineering type work on the SnO electrodes that has to be carried out in order to make the SnO material useful for rechargeable Li battery application.

IV. Summary and Conclusion

SnO nanoparticles could be synthesized quite easily in a one-step reaction from very cheap and simple precursors using sonochemical methods. The product thus formed is amorphous and could be transformed to a nanocrystalline phase by heating to 200 °C. Both the amorphous and the nanocrystalline SnO are electrochemically active and can be reduced in nonaqueous Li salt solutions to matrixes of Li_2O and $Li_{17}Sn_4$. The possible use of these materials as the active mass of anodes for rechargeable Li batteries was examined. We found that the nanocrystalline SnO is superior as an anode material over the amorphous and microcrystalline phases. Its reversible capacity in lithiation−delithiation processes reaches the theoretical one, 790 mAh/g, corresponding to the formation of a $Li_{17}Sn_4$ compound. The behavior of electrodes comprised of this material (and any other type of SnO as well) depends on a variety of critical parameters, which relate to the composite structure of the electrodes and the electrolytic solutions. These include the type of conductive additive, its percentage, the percentage of the binder in the composite electrode, and the electrode's porosity (attenuated by the application of pressure during its preparation). Two irreversible processes accompany lithiation of SnO: formation of Li_2O and reduction of solution species, which form passivating surface films. The performance of SnO anodes depends largely on the properties of these surface films. Three major processes influence the impedance of the lithiated SnO electrodes: lithium ion migration through the surface films, charge transfer at the surface film/active mass interface, and solid-state diffusion of lithium in the $Li_{17}Sn_4$ compound. It should be emphasized that the irreversible capacity of SnO electrodes, which is higher than their reversible capacity (>900 mAh/g), is unacceptable for battery application (in which the lithium source is usually the Li_xMO_y cathode, M is a transition metal, like Mn, Co, Ni, V). In addition, upon charge−discharge cycling (repeated lithiation−delithiation processes), the capacity gradually fades. This capacity fading is connected to morphological changes in the composite electrodes appearing as cracks in the active mass. These changes are probably related to repeated volume changes of the active mass as Li is inserted (increase) and deinserted (decrease), which are accompanied by obvious surface reactions between the $Li_{17}Sn_4$ and solution species. When the morphology is not stable, there is no way to stabilize the electrode−solution interfaces and to avoid continuous surface reactions between the lithium−tin compounds and solution species. We suggest that, by a proper choice of binder and conductive additives, it is possible to reduce the capacity fading of anodes comprised of nanoscopic SnO. The very high theoretical capacity of this material, that can indeed be reached practically, leaves enough room for the use of various types of additives in the composite electrodes, in addition to the active mass.

The last point of interest to be mentioned is a comparison between the behavior of the SnO electrodes described herein and the behavior of nanocrystalline and nanoamorphous SnO_2 (also synthesized by sonochemistry) described previously.[24] In general, the irreversible capacity of SnO_2 electrodes was much higher than that of the SnO electrodes, due to an additional irreversible process that forms two Li_2O molecules upon the full lithiation of SnO_2. In addition, the reversible capacity obtained with nanocrystalline SnO_2 electrodes was lower than that of nanocrystalline SnO electrodes. However, the capacity of the amorphous SnO_2 electrodes was 1 order of magnitude higher than that of the amorphous SnO ones. The stability of the SnO_2 electrodes in repeated lithiation−delithiation cycling was also higher than that of SnO electrodes. Hence, we can suggest that the fact that lithiated SnO_2 electrodes contain a higher Li_2O content than lithiated SnO has a positive impact on the stabilization and integrity of the $Li_{17}Sn_4$ phase embedded in the Li oxide matrix. This point definitely warrants further study.

Acknowledgment. Partial support for this work was obtained from the BMBF, the German Ministry of Science, in the framework of the DIP Program for Collaboration between Israeli and German Scientists and from the EC under contract number EKN6-CT-200100509.

CM021137M